Mon. Not. R. Astron. Soc. **000**, 000–000 (0000) Printed 20 January 2014 (MN LATEX style file v2.2)

Non-parametric method for mass modelling spherical systems

P. Steger[1⋆], D. von Rickenbach[1], J. I. Read[1,2]
[1] *Institute for Astronomy, Department of Physics, ETH Zürich, Wolfgang-Pauli-Strasse 27, CH-8093 Zürich, Switzerland*
[2] *Department of Physics, University of Surrey, Guildford, GU2 7XH, UK*

20 January 2014

ABSTRACT

We propose a new non-parametric method to determine the mass distribution in spherical systems. A high dimensional parameter space encoding tracer density, line of sight velocity dispersion and total mass density is sampled with a MultiNest parameter space explorer.

Without assumptions on the functional form of any of these profiles, we can reproduce liably the total mass density of mock dwarf galaxies, and disentangle the degeneracy between dark matter density and tracer velocity anisotropy.

We show early applications to observed dwarf galaxies, and point out what data quality is required to detect cores of radius r_c.

Key words: galaxies: dwarf – galaxies: fundamental parameters – galaxies: kinematics and dynamics – cosmology: dark matter

1 INTRODUCTION

Cosmological ΛCDM simulations of representative patches of the Universe predict the dark matter to assemble self-similarly.

Assuming that only dark matter might influence the physics on all scales down to the stellar regime, Navarro et al. (1997) found that the density profiles of the resulting halos are best described by a function diverging as r^{-1} towards the center. Given that only a finite amount of dark matter is available in the halo, there exists a very small lower bound for a turnover radius, where the density approaches a constant value.

Observations of low surface brightness galaxies measure rotation curves and deduce from them a constant density below a rather large scale radius r_S (de Blok et al. 2001), (McGaugh et al. 2001), contrary to the theoretical predictions. This fact became known as the cusp/core problem.

Many solutions have been proposed to solve it. It was deemed possible that difficulties in data modelling prevent observations from resolving cusps.

From a theoretical point, it was proposed that dark matter is not cold as assumed, with a warm component smearing out density peaks below a certain scale.

Dark matter could also be self-interacting, as e.g. postulated by (Spergel & Steinhardt (2000), Vogelsberger et al. (2012)), and have a large scattering cross-section and low annihilation or dissipation cross-section, and thus prevent formation of overly-dense cusps.

For the simulations in question, it became clear that baryonic physics plays a crucial role for the buildup of the overall density profile on small scales, and thus dark matter.

In particular, modelling of stellar feedback, the introduction of a higher density threshold for star formation and an increase of resolution for treatment of individual star-forming regions in a cosmological context led simulations to reveal dwarf galaxies with shallow central density slopes in dark matter (Governato et al. 2010). This compares well with what is found in THINGS dwarf galaxies (Oh et al. 2011).

Another type of dwarf galaxies, the dwarf spheroidals, lie closer to the Sun and can be resolved much better, often allowing us to observe individual stars. We need a method to model their mass distribution from the observations to investigate whether they exhibit a cusp or a core, and whether simulations are able to reproduce the dark matter distribution.

An early approach for general triaxial systems in dynamical equilibrium was proposed by Schwarzschild (1979): Based on a density profile and a corresponding gravitational potential, an ensemble of orbits are calculated and superposed to yield the underlying density profile.

Another method makes use of the Jeans equations encompassing tracer density, velocity dispersion and the gravitational potential to solve for the potential, and ultimately get the underlying dark matter density (Binney & Tremaine 2008). Mostly, a functional form with some free parameters

⋆ E-mail: psteger@phys.ethz.ch

is assumed for the density profile, and fitting routines are used to yield the best agreeing form.

Another assumption is required for the velocity anisotropy profile to get a mass density in the case of lowest-order Jeans equations. Since it is not known a priori and hard to measure observationally how much the system is supported by rotational motion, this leads to a degeneracy between mass and velocity anisotropy.

Higher order Jeans equations can help to break this degeneracy (Łokas 2002). Another degeneracy between inner DM slope and concentration shows up, though. With better data available for the local dSphs, distribution function based methods may be used.

Yet another approach is to use the motion of globular clusters inside dwarf galaxies (Goerdt et al. 2006), (Cole et al. 2012). If the density distribution follows a cored profile, globular clusters will not fall in, or will even get pushed out of the core if they formed inside. In Fornax dSph, there is evidence for a core (Read et al. 2006).

Walker & Peñarrubia (2011) split the stellar tracers into two populations with different metallicities and half-mass radii, and make use of the fact that the enclosed mass at the half-mass radius is independent of the underlying velocity anisotropy profile, to get two points in the center of the dwarf galaxy, from which constraints on the inner DM density slope can be drawn.

We want to get the full density profile, though.

In this paper, we propose a new non-parametric mass-modelling technique based on the Jeans approach, with no assumptions on the functional form of the dark matter density, nor the velocity anisotropy profile.

We assume spherical symmetry in a first step. Beware that dSph galaxies of the local group are known to be slightly non-spherical, with an average ellipticity of 0.3 (Mateo 1998).

Our method has following advantages over other methods presented so far:

(i) no assumptions on the functional form of the underlying dark matter;

(ii) applicable to any gravitational model, since Jeans equation and Poisson equation are solved each on their own;

(iii) robust to noise in the data, as no numerical differentiation is used as soon as the three-dimensional density model is set up.

2 METHOD

The collisionless Boltzmann equation for a spherical system with gravitational potential Φ,

$$\frac{\mathrm{d}f}{\mathrm{d}t} = \frac{\partial f}{\partial t} + \nabla_{\vec{x}} f \cdot \vec{v} - \nabla_{\vec{v}} f \cdot \nabla_{\vec{x}} \Phi = 0, \tag{1}$$

describes the motion of tracer stars with distribution function $f(\vec{x}, \vec{v})$.

In spherical coordinates (r, θ, ϕ), the collisionless Boltzmann equation then reads as

$$\frac{\partial f}{\partial t} + \dot{r}\frac{\partial f}{\partial r} + \dot{\theta}\frac{\partial f}{\partial \theta} + \dot{\phi}\frac{\partial f}{\partial \phi} + \dot{v}_r\frac{\partial f}{\partial v_r} + \dot{v}_\theta\frac{\partial f}{\partial v_\theta} + \dot{v}_\phi\frac{\partial f}{\partial v_\phi} = 0 \tag{2}$$

with velocities

$$\dot{r} = v_r, \tag{3}$$

$$\dot{\theta} = v_\theta / r \tag{4}$$

$$\dot{\phi} = v_\phi / r \sin\theta. \tag{5}$$

The assumption of steady state hydrodynamic equilibrium gives $\partial f/\partial t = 0$ and $\bar{v}_r = 0$, and using spherical symmetry $\bar{v}_\theta = 0$, $\bar{v}_\phi = 0$, with a unique tangential velocity dispersion $\sigma_\phi^2 = \sigma_\theta^2 = \sigma_t^2$ and a fourth order moment $\bar{v_r^4}$ we get

$$\frac{1}{\nu}\frac{\partial}{\partial r}(\nu\sigma_r^2) + 2\frac{\sigma_r^2 - \sigma_t^2}{r} = -\frac{\partial \Phi}{\partial r} = -\frac{GM(<r)}{r^2}, \tag{6}$$

$$\frac{\partial}{\partial r}(\nu\bar{v_r^4}) + \frac{2\beta}{r}\nu\bar{v_r^4} + 3\nu\sigma_r^2\frac{\partial \Phi}{\partial r} = 0, \tag{7}$$

with enclosed mass $M(<r)$, gravitational constant $G = 6.67398 \cdot 10^{-11}\mathrm{m}^3/\mathrm{kg\,s}^2$. The departure from spherical hydrostatic equilibrium $\sigma_r^2 = \sigma_t^2$ is measured by the anisotropy parameter

$$\beta \equiv 1 - \frac{\sigma_t^2}{\sigma_r^2} \tag{8}$$

with values in the range from $-\infty$ (purely circular orbits) through 0 (hydrostatic equilibrium) to 1 (purely radial orbits).

Integrating both sides of equation 6 gives the main equation of this paper,

$$\sigma_r^2(R) = \frac{1}{\nu(R)} \exp\left(-2\int_{r_{min}}^{R} \frac{\beta(s)}{s}\mathrm{d}s\right) \cdot \tag{9}$$

$$\int_R^\infty \frac{GM(r)\nu(r)}{r^2} \exp\left(2\int_{r_{min}}^{r} \frac{\beta(s)}{s}\mathrm{d}s\right)\mathrm{d}r.$$

$$\bar{v_r^4}(R) = \frac{3}{\nu(R)} \exp\left(-2\int_{r_{min}}^{R} \frac{\beta(s)}{s}\mathrm{d}s\right) \cdot$$

$$\int_R^\infty \frac{GM(r)\nu\sigma_r^2}{r^2} \exp\left(2\int_{r_{min}}^{r} \frac{\beta(s)}{s}\mathrm{d}s\right)\mathrm{d}r.$$

For distant spherical systems, only the projected velocity dispersion σ_{LOS} and the fourth order moment $\bar{v_{\mathrm{los}}^4}$ can be measured, which in our case is given by

$$\sigma_{\mathrm{LOS}}^2(R) = \frac{2}{\Sigma(R)}\int_R^\infty \left(1 - \beta\frac{R^2}{r^2}\right)\frac{\nu(r)\sigma_r^2(r)r}{\sqrt{r^2 - R^2}}\mathrm{d}r, \tag{10}$$

$$\bar{v_{\mathrm{LOS}}^4} = \frac{2}{\Sigma(R)}\int_R^\infty \frac{\nu\bar{v_r^4}r}{\sqrt{r^2 - R^2}} g(r, R, \beta)\mathrm{d}r \tag{11}$$

$$g(r, R, \beta) = 1 - 2\beta\frac{R^2}{r^2} + \frac{\beta(1+\beta)}{2}\frac{R^4}{r^4}$$

where $\Sigma(R)$ denotes the surface mass density at radius R.

As in Łokas et al. (2005), we will compare the kurtosis

$$\kappa_{\mathrm{LOS}} = \frac{\bar{v_{\mathrm{LOS}}^4}}{\sigma_{\mathrm{LOS}}^4}$$

between data and our model.

In the following, we present a non-parametric method for the solution of equation 10 for the total gravitating mass density $\rho(r)$, given observed $\nu(r)$ and $\sigma_{\rm LOS}(r)$, where r denotes the projected two-dimensional radius from the center of mass of the spherical system. We get the enclosed mass $M(<r)$ from the density via

$$M(<r) = \int_0^r \rho(r) r^2 {\rm d}r, \tag{12}$$

which shows up in eq. 9. In principle, the method can be generalized to investigate alternative gravity models, if the acceleration $GM(r)/r^2$ is replaced with the respective form of $-\partial\Phi/\partial r$.

The degeneracy between mass M and velocity anisotropy β is accounted for: For any non-isothermal system, we let vary the anisotropy $\beta(r)$ as well. We checked that in the case of a simple Hernquist profile, $\beta(r) \approx 0$ is retrieved correctly.

We sample the parameter space $[\nu_i, \sigma_{{\rm LOS},i}, \rho]$ for distinct populations $i = 1...N$ of stellar or gaseous tracers with a Monte Carlo Markov Chain method.

Early approaches were performed with a custom MCMC method. It proved unfeasible to sample the whole parameter space on human timescales due to its high dimensionality.

To circumvent many likelihood evaluations around a local minimum, we changed the underlying sampling method to use several MCMC walkers, along the lines recently described in (**?**) for their parallel code RUN DMC to analyze radial velocity observations of planetary systems.

A useful framework was found in MultiNest (Feroz et al. (2009)), which is a Bayesian nested sampling algorithm to generate posterior samples from non-trivial distributions in high dimensions.

There are a large number of parameters from the representation of the radial profiles of each of those in N_{bin} bins, with only very few constraints from physical priors. The functional form of the profiles is not predescribed. This is what we call *non-parametric*.

MultiNest samples the n-dimensional hypercube $\kappa = [0,1]^n$, which needs to be translated into physical prior distributions for each of the parameter profiles:

The overall density ρ is represented in terms of the logarithmic density slopes $n(r_i) = \kappa_{\rho_i} = (\kappa_{\rho_i})$, $1 \leqslant i \leqslant N_\rho + 3$ and calculated as

$$\rho(r) = \rho(r_{1/2}) \cdot \exp\left[\int_{r_{1/2}}^r n(s){\rm d}\right] s,$$

with the density at half-light radius $\rho(r_{1/2}) =$, and $n(r)$ interpolated linearly in between bin radii $r_{i-1} < r < r_i$. We prescribe two additional slopes $n_0 < -3, n_\infty > -3$ for the asymptotic density slopes towards $r = 0$ and $r = \infty$, which are reached at half the smallest and twice the largest bin radius.

The velocity anisotropy β is allowed to vary freely in the interval $[0, \infty[$ by sampling the modified, symmetric β_* (**(TODO: cite Read)**),

$$\beta_* = \frac{\sigma_r^2 - \sigma_t^2}{\sigma_r^2 + \sigma_t^2} = \frac{\beta}{2-\beta} \in [-1, 1]$$

with a polynomial s.t.

$$\beta_*(r) = \sum_i = 0^{N_\beta} \kappa_{\beta_i} \cdot \left(\frac{r_i}{r_{\rm max}}\right)^i,$$

where $\kappa_{\beta_i} \in [0,1]$. With this method, unphysical $\beta > 1$ are possible, which we prevent with a correction

$$\beta_*(r_i) := \min(\max(\beta_*(r_i), -1), 1).$$

This approach allows us to change the number of parameters N_β easily, and to sample many qualitatively different models – isotropic, radially biased, tangentially biased, and any gentle transitions between those – with very few parameters.

In a next step, $\sigma_{{\rm LOS},i}(r)$ is calculated from $\nu(r)$, $\rho(r)$, and $\beta(r)$ according eq. 10. This is done numerically, involving three integrations, which are performed with polynomial extrapolations of the integrands up to infinity, s.t. missing contributions from $r > r_{max}$ do not lead to an artificial falloff of $\sigma_{\rm LOS}$. The additional parameters of the slopes are calculated from the values at lower radii, thus preventing the introduction of any further parameters.

The last step involves comparison of the projected $\nu_i(r)$, $\sigma_i(r)$ and $\beta_i(r)$, if available, to the data for the tracer populations to get a likelihood based on the overall goodness of fit

$$\chi^2 = \sum_{i=1}^N \chi^2_{\nu,i} + \chi^2_{\sigma,i} + \chi^2_{\beta,i} \tag{13}$$

$$\chi^2_{\nu,i} = \sum_{j=1}^{N_{bin}} \left(\frac{\nu_{i,{\rm data}}(r_j) - \nu_{i,{\rm model}}(r_j)}{\epsilon_\nu(r_j)}\right)^2. \tag{14}$$

and accordingly for $\chi^2_{\sigma,i}$ and $\chi^2_{\beta,i}$. In absence of a measured $\beta_i(r)$, we set $\chi^2_{\beta,i} = 0$.

2.1 Binning characteristics

The number of bins for ρ, ν_i, β_i, and σ_i are free parameters. They are set to fulfill

$$n_\nu = n_\sigma = n_\beta = n_\rho \leqslant n_{\rm data} \tag{15}$$

with number of datapoints $n_{\rm data}$. This choice simplifies integration greatly, and prevents invention of information on scales smaller than the frequency of datapoints.

(TODO: check that nbin is set s.t.)

$$\chi^2_{red} = \frac{\chi^2}{n_{\rm data} - n_\nu - n_\sigma - n_\beta - n_\rho - 1} \tag{16}$$

is minimized, and still the whole parameter space is tracked.

The whole parameter space for β_i is sampled with $n_\beta = 12$ if $n_{\rm data} = 30$ in the case of 10000 tracers.

The dark matter density is calculated by subtracting the measured baryon density from the dynamical mass density.

2.2 Priors

Following priors are included in the model, and help to reject unphysical samplings from the start:

1) baryon prior: $\rho(r) \geqslant \rho_b(r) - \epsilon_{\rho,b}(r) \forall r \geqslant 0$, ensures that no models with overall densities below the measured baryon density are considered any further;
2) mass restriction: $M(r > r_{max}) \leqslant M(< r_{max})/3.$, rejects any model which has more than $M_\infty/3$ in the extrapolated bins;
3) $\beta_i(r + \Delta r) - \beta_i(r) < 0.5$: prevent any sudden jumps in β_i;

We show in the appendix what effects the disabling of these priors have.

3 RESULTS

We apply our method to a set of mock data, the spherical models for the Gaia challenge by Walker and Penarrubia. They consist of dynamical tracer populations with density distribution

$$\nu_*(r) = \nu_0 \left(\frac{r}{r_*}\right)^{-\gamma_*} \left[1 + \left(\frac{r}{r_*}\right)^{\alpha_*}\right]^{(\gamma_* - \beta_*)/\alpha_*} \tag{17}$$

inside dark matter halos of the form

$$\rho_{\rm DM} = \rho_0 \left(\frac{r}{r_{\rm DM}}\right)^{-\gamma_{\rm DM}} \left[1 + \left(\frac{r}{r_{\rm DM}}\right)^{\alpha_{\rm DM}}\right]^{(\gamma_{\rm DM} - \beta_{\rm DM})/\alpha_{\rm DM}} \tag{18}$$

with scale radii $r_*, r_{\rm DM}$, inner and outer logarithmic slopes of $\gamma_*, \gamma_{\rm DM}$ and $\beta_*, \beta_{\rm DM}$, with transition parameters $\alpha_*, \alpha_{\rm DM}$.

The anisotropy follows the functional form of **?** and **?**,

$$\beta_{\rm anisotropy}(r) = 1 - \frac{\sigma_\theta^2}{\sigma_r^2} = \frac{r^2}{r^2 + r_a^2}. \tag{19}$$

with scale radius r_a, turning over from nearly isotropic at $r \to 0$ to radially biased at $r_* = r_a$.

Of these distributions, finite samplings are taken and converted to mock observational data including observational parameters like spectral indices, systemic velocities, proper motions, and binary motion.

(TODO: mention Gaia challenge)

3.1 Cusps and Cores

Applied on a profile with a cusp in the DM density profile, our method reproduces the density profile (fig. 1).

Fitted $\nu(r)$ and $\sigma_{\rm LOS}$ are shown in fig. 2.

Introducing κ_i in the χ^2 did **(TODO: not?)** result in a change of behavior for the velocity anisotropy parameter.

(TODO: observations for kurtosis) (TODO: better/worse fitting of density)

3.2 Cored Model

For a cored profile, we have a similar result, see fig. 3. **(TODO: rerun)**

3.3 Triaxial mock data

(TODO: motivation: triaxiality of observed dwarfs, effects from other mass modelling schemes)

The models were generated with a Made 2 Measure algorithm of **?** and are tailored to follow a similar profile to the profiles specified above for the dwarf galaxies. They show a density profile of

$$\rho(r) = \frac{\rho_S}{\left(\frac{r}{r_S}\right)^\gamma \left(1 + \left(\frac{r}{r_S}\right)^{1/\alpha}\right)^{\alpha(\beta-\gamma)}} \tag{20}$$

with radius r, scale radius $r_S = 1.5$kpc, $\alpha = 1$, $\beta = 4$. For the cusped profiles we have an inner logarithmic slope of $-\gamma = -1$, scale density $\rho_S = 5.522 \cdot 10^7 M_\odot/\text{kpc}^3$, and $M_{\rm tot} = 1.171 \cdot 10^9 M_\odot$, while for the cored one we have $\gamma = 0.23$, $\rho_S = 1.177 \cdot 10^8 M_\odot$, $M_{\rm tot} = 1.802 \cdot 10^9 M_\odot$. The axis ratios are $b/a = 0.8$ and $c/a = 0.6$. The stars have negligible mass and follow the same functional form in the density profile as dark matter, with $\alpha = 0.34, \beta = 5.92, \gamma = 0.23, r_S = 0.81$kpc.

The velocity anisotropy of the stellar part is calculated via

$$\beta(r) = \frac{r_{s,\beta}^\eta \beta_0 + r^\eta \beta_\infty}{r^\eta + r_{s,\beta}^\eta}, \tag{21}$$

with $r_{s,\beta} = 0.81$kpc, $\beta_0 = 0$, $\beta_\infty = 0.5$ and $\eta = 0.5$, going from isotropic to radially anisotropic with increasing radius.

The retrieved density profile (fig. 4) is constantly overestimating the density.

(TODO: other projections) (TODO: reason: projection)

4 CONCLUSIONS

(TODO: code reproduces mock data)
(TODO: better with cores/cusp)
(TODO: influences of parameters)
(TODO: minimum data quality needed)

5 ACKNOWLEDGEMENTS

JIR would like to acknowledge support from SNF grant PP00P2_128540/1.

REFERENCES

Binney J., Tremaine S., 2008, Galactic Dynamics: Second Edition. Princeton University Press
Cole D. R., Dehnen W., Read J. I., Wilkinson M. I., 2012, MNRAS, 426, 601

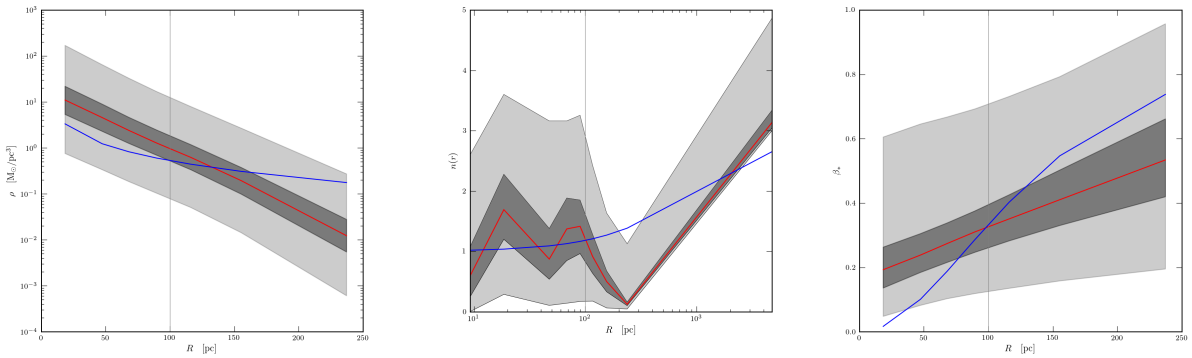

Figure 1. Reconstructed density, density slope, and velocity anisotropy of a cusped model (red shows median, shaded areas are 68 and 95 percentiles) for 10^4 tracer particles, for $3 \cdot 10^5$ models. The blue curve shows the underlying theoretical model. The half-light radius of all stellar tracer particles is depicted as gray vertical line.

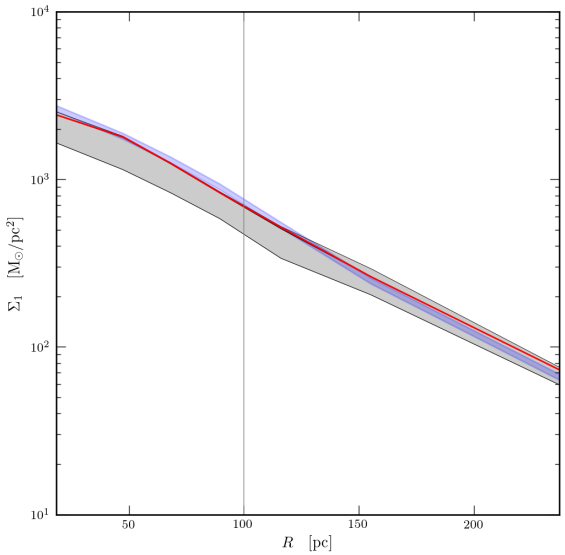

Figure 2. Fitted $\nu(r)$ and $\sigma_{\rm LOS}(r)$ for the stellar components in the cusped profile of fig. 1.

de Blok W. J. G., McGaugh S. S., Rubin V. C., 2001, AJ, 122, 2396
Feroz F., Hobson M. P., Bridges M., 2009, MNRAS, 398, 1601
Goerdt T., Moore B., Read J. I., Stadel J., Zemp M., 2006, MNRAS, 368, 1073
Governato F. et al., 2010, Nature, 463, 203
Łokas E. L., 2002, MNRAS, 333, 697
Łokas E. L., Mamon G. A., Prada F., 2005, MNRAS, 363, 918
Mateo M. L., 1998, ARA&A, 36, 435
McGaugh S. S., Rubin V. C., de Blok W. J. G., 2001, AJ, 122, 2381
Navarro J. F., Frenk C. S., White S. D. M., 1997, ApJ, 490, 493
Oh S.-H., Brook C., Governato F., Brinks E., Mayer L., de Blok W. J. G., Brooks A., Walter F., 2011, AJ, 142, 24
Read J. I., Pontzen A. P., Viel M., 2006, MNRAS, 371, 885
Schwarzschild M., 1979, ApJ, 232, 236
Spergel D. N., Steinhardt P. J., 2000, Physical Review Letters, 84, 3760
Vogelsberger M., Zavala J., Loeb A., 2012, MNRAS, 423, 3740
Walker M. G., Peñarrubia J., 2011, ApJ, 742, 20

Figure 3. A cored profile: Reconstructed mass of the MCMC model (red shows median, shaded areas are 68 and 90 percentiles) for 10^4 tracer particles based on $3 \cdot 10^5$ sampled models. The blue curve shows the underlying theoretical model.

(TODO: redo triaxial model)

Figure 4. Density profile of a triaxial mock dwarf, for which the line of sight is inclined with 45 degrees with respect to all axes.